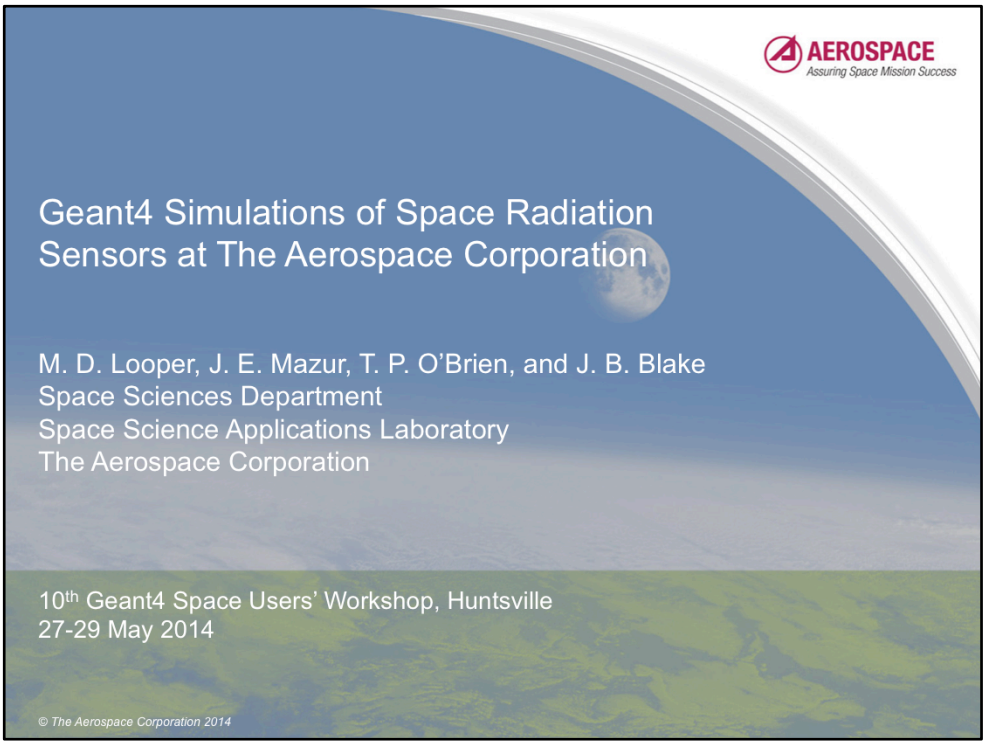


The Aerospace Corporation is a non-profit company that exists mostly to serve the U.S. Air Force space program, and also works with civilian and commercial space programs. SSAL's part in "Assuring Space Mission Success" includes evaluation of radiation hazards to spacecraft and astronauts; my part of that includes calculating radiation dose under shielding, electrostatic charge deposition, and other applied-physics problems, for which Geant4 is my main tool. However, none of those calculations are valuable without knowledge of the space radiation environment that causes the phenomena, and we also design, build, and fly sensors to make measurements of this. In this talk I will discuss three recently launched sensors for which I've done a substantial amount of modeling and data analysis, again with Geant4 as a critical tool. My intent here is to show the Geant4 team some of the capabilities in the code that I have found to be particularly important for this kind of work.

## Recent Space Missions and Radiation Sensors

- Cosmic Ray Telescope for the Effects of Radiation (CRaTER)
  - *Launched June 2009 aboard Lunar Reconnaissance Orbiter (LRO)*
  - *Nominal mapping orbit is circular at 50 km altitude, polar*
  - *Purpose is to measure energy deposit spectra under shielding*
- Relativistic Proton Spectrometer (RPS)
  - *Launched August 2012 aboard Radiation Belt Storm Probes (RBSP)*
    - After launch, renamed Van Allen Probes
  - *Two S/C in near-equatorial, elliptical Earth orbits out to 5.8 Earth radii*
  - *Sensor to measure protons up to GeV in heart of Inner Van Allen Belt*
- Magnetic Electron Ion Spectrometer (MagEIS)
  - *Also aboard Van Allen Probes*
  - *Focus here on electron sensors, tens of keV to several MeV*



AEROSPACE

## CRaTER Sensor Head

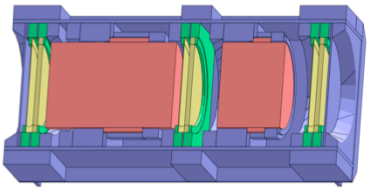

To space ← → To moon

- Six silicon solid-state detectors
- Thick detectors measure low LET and thin detectors measure high
- Two cylinders of A-150 Tissue Equivalent Plastic in stack

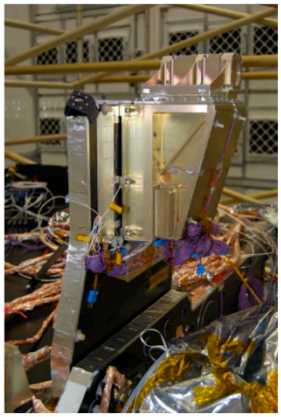

Photo courtesy of NASA

3

AEROSPACE

CRaTER is designed to measure not the composition and spectra of incident particles (although it can do that, to some extent), but rather the effects of that radiation: the spectra of energy deposit events behind shielding, which is designed to represent the muscle tissue over an astronaut's radiation-sensitive bone marrow. The three pairs of detectors, if required to be triggered in coincidence, define a collimated "beam" of incident particles with a well-defined amount of shielding overlying each detector.

## Observations During Recent Solar Minimum

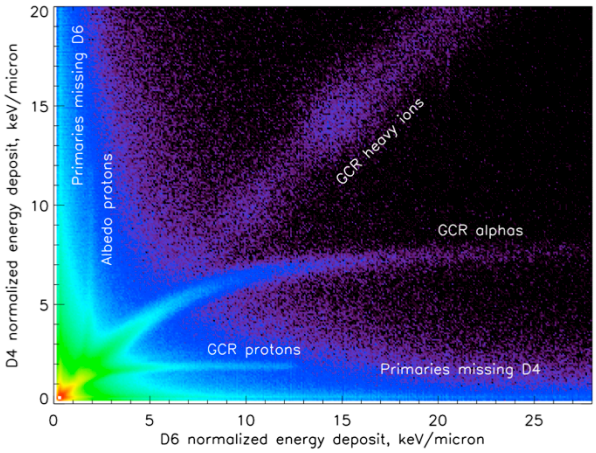


*Looper et al., Space Weather 2013*

4

AEROSPACE

This is a sample of energy-deposit events for coincidences between thick detectors D4 and D6, with D2 not triggered and thin detectors ignored, and with a six-decade logarithmic color scale, during the recent record-setting fluxes of galactic cosmic rays (GCRs) at the height of solar minimum early in the mission (mid-2009 to early 2010). Bands of events with identifiable source species are labeled, and summing up their energy deposits in one of the detectors gives their contribution to the dose received under its particular amount of shielding. However, there is a background due to primary particles that miss one or the other detector, but that send off a knock-on electron (a.k.a. delta ray) that triggers a valid coincidence remotely by striking the other detector. These out-of-aperture events will contaminate the collimated sample desired, and must be understood and corrected for.

## Geant4 Simulations of Lunar GCR Secondaries

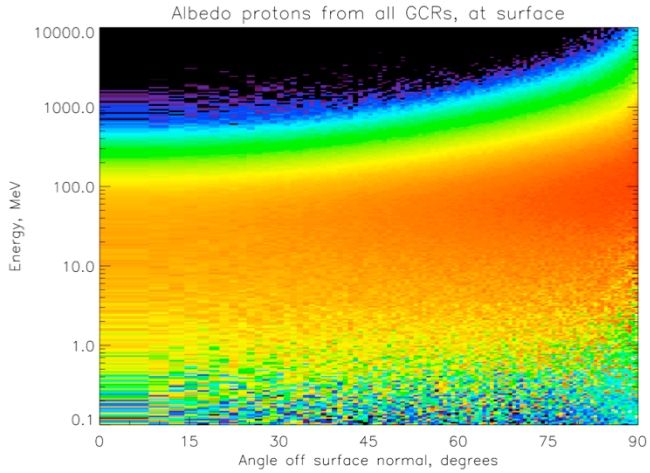


5

AEROSPACE

To do this, we start by modeling the secondary ("albedo") particles produced by impact of GCRs on the lunar surface. A twenty-meter slab of 3 gm/cc ferroan anorthite is isotropically illuminated by GCR ions, and both particles coming off the surface and particles reaching a "counting sphere" at 50 km altitude are tabulated. This plot (six-decade logarithmic color scale) is for protons; a relatively soft, isotropic flux comes more or less straight up, presumably from decay of target nuclei excited by GCR impact, while the flux hardens and intensifies toward the limb (90 degrees) as forward-scattered fragments from nuclear collisions due to glancingly-incident GCR nuclei travel sideways and up rather than down. This pattern in energy and angle holds for most secondary species.

## Contribution to Albedo Protons Due to Heavy GCRs

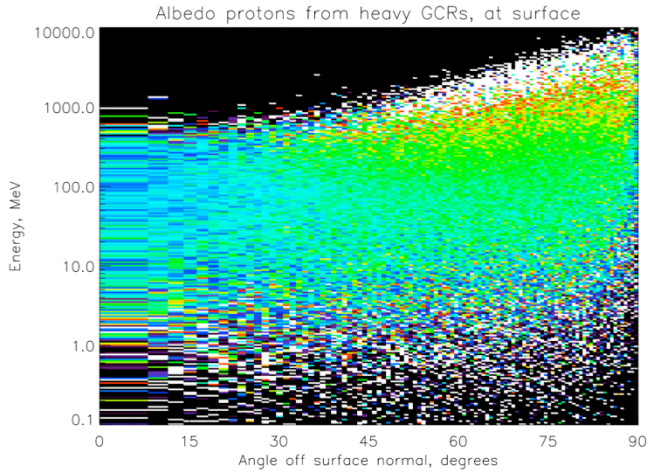


6

AEROSPACE

Since the last Geant4 Space Users' Workshop, we have added the physics of nuclear interactions between heavy ion projectiles and heavy target nuclei to our simulations of both the sensor response and the lunar albedo particle production (version 9.6, Shielding_LIV physics list). This is a plot of the ratio between the albedo protons due to GCR primaries heavier than helium and the albedo protons due to GCR proton primaries; color scale is linear, from 0 to 0.1. Black/white checkered regions are where statistics are poor at the fringes of the band in the previous plot; however, in the main band it can be seen that while heavy GCRs produce relatively few protons (and albedo particles generally) coming nearly straight up, there is about a 10% enhancement at higher energies toward the limb (GCR helium produces about three times this effect). Modeling/observation comparisons to date have focused on upgoing albedo, where there is little effect, since that's how the spacecraft is oriented most of the time; the spacecraft does sometimes point our sensor closer to or over the limb, and we are preparing to compare that data with observations. We should be able to see the difference made by contributions to the more energetic albedo protons coming from the limb from heavy ion GCRs.

## Effect of Water in Regolith on Lunar Albedo Protons

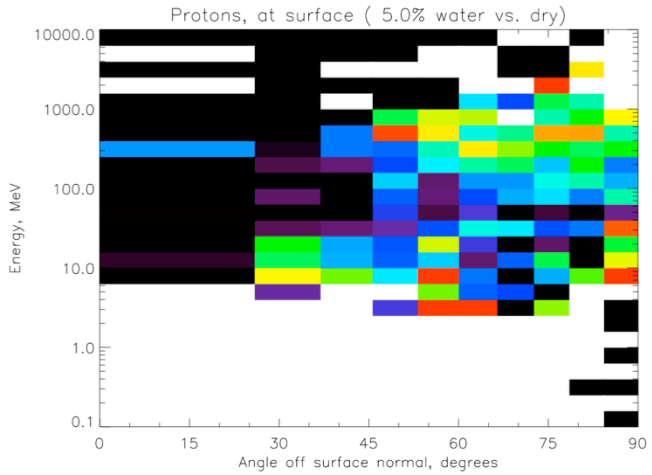


7

AEROSPACE

We have also modeled the effect of water or ice mixed with the lunar regolith on lunar albedo, to test our sensor's ability to detect it. This is a difference plot between albedo protons due to GCR protons striking (very) moist regolith vs. dry, saturating at plus or minus 1%. Binning had to be coarsened to build up statistics; nonetheless it can be seen that water at this level depresses upward albedo protons by about 1% and enhances higher energy protons from the limb at about 0.5% (the effect should be linear with the amount of water). We are still evaluating whether, with a sufficiently long "exposure," we could detect reasonable amounts of water in the regolith.

## Cosmic Ray Albedo Neutron Decay (CRAND)

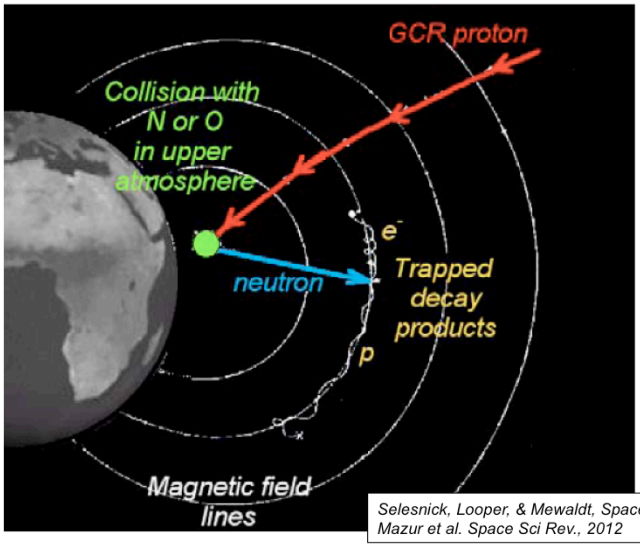


*Selesnick, Looper, & Mewaldt, Space Weather 2007*
*Mazur et al. Space Sci Rev., 2012*

8

AEROSPACE

A related problem is to calculate the production of secondary particles, especially neutrons, by GCR primaries striking the Earth's atmosphere. When neutrons decay in flight as they pass through the Earth's magnetic field, the resultant proton can become trapped by the field for very long periods; this "CRAND" process is the source of the Earth's inner Van Allen Belt. We used Geant4 versions 6.2 to 8.0 to model this process, and the results were incorporated in a new model of the Inner Zone (Selesnick, Looper, & Mewaldt, 2007). We are getting ready to redo the simulation with version 10.0, and also to model the response to hydrogen and helium isotopes of the Proton/Electron Telescope aboard the long-lived SAMPEX satellite (1992-2012); the sensor has negligible neutron sensitivity, but comparisons of its observations with predicted albedo fluxes of these species will be used to validate the new albedo model.

## Relativistic Proton Spectrometer (RPS)

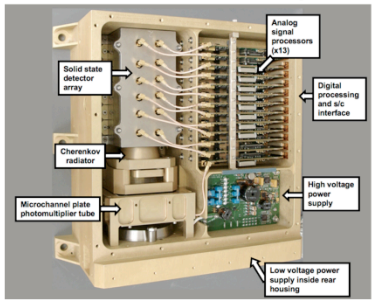


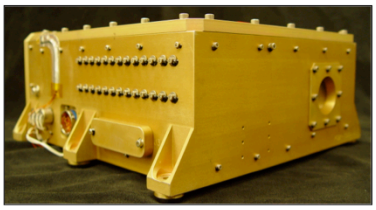

Mazur et al., Space Sci Rev, 2012

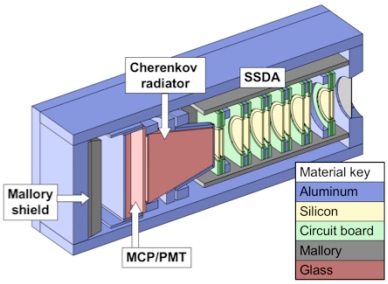


- Real sensor images at left, Geant4 above
- Designed for maximum background rejection
- Four 20mm diameter Si SSDs for collimation
- Eight 23mm SSDs to measure energy deposit
- Cherenkov radiator assembly (CRA) with MCP
  - *Black paint on small end*
  - *Shaped for directional total internal reflection*

9

AEROSPACE

RPS is a spectrometer designed to measure relativistic protons up to 1 GeV in the intense radiation environment of the heart of the inner Van Allen Belt. Larger energy-deposit SSDs reduce edge effects for particles traveling through smaller collimation SSDs; radiator shape and paint suppress light from backward-going protons to improve directionality in penetrating-proton environment. At the last Space Users' Workshop, we discussed modeling we had done to support calibration work at the TRIUMF particle accelerator; since then we have acquired enough experience with the flight data to revisit our calibrations, not least because the natural GCR and trapped protons extend to higher energies than we were able to obtain on the ground.

## Observations, Cherenkov vs. SSD

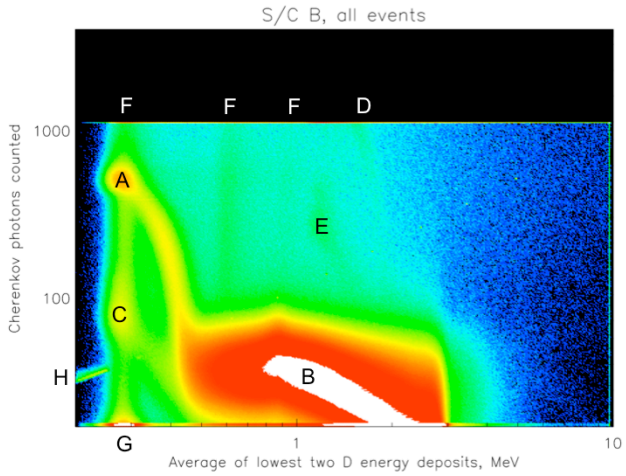


A: High-energy forward protons

B: Protons below Cherenkov threshold, with scintillation and delta rays in CRA

C: High-energy backward protons

D: Forward alphas

E: Backward alphas

F: Delta rays from protons missing SSDs

G: Trapped electrons

H: Calibration pulser



AEROSPACE

Simulations that track individual particles through the stack, as well as energy deposits and CRA light, enable us to identify additional populations not part of the main (forward proton) response, which we will try to eliminate with cuts.

## Observations and Simulations, SSDs 1 vs. 8

Observations, S/C B, cuts on CRA vs. min 2 SSD

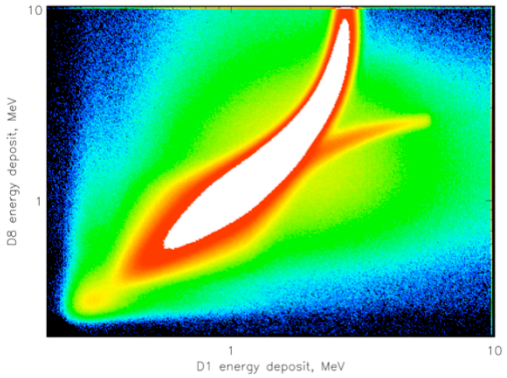


Simulations, forward protons

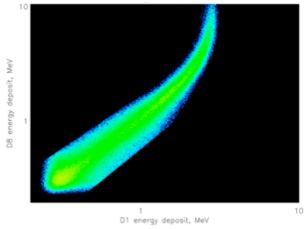


Simulations, backward protons

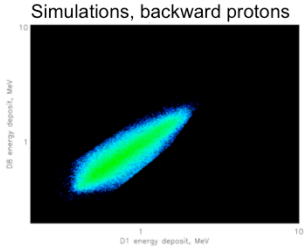


- Even with cuts on CRA vs. SSD, “spur” remains above
- Cut on pairs of SSDs to eliminate these backward protons
- Simulations at right show particles surviving all cuts



AEROSPACE

Applying a cut to select the valid region on the previous slide’s plot, we still see a “spur” to the right in a plot of energy deposits in two detectors. Applying cuts in D8 vs. each of D1-D7, and another cut on the curvature between pairs of detectors, we get a clean track in simulation of events with a single proton going forward through the stack (upper right); however, we are not able to eliminate all events with a backward-going proton (lower right) in the middle energy range between the “spur” (low energy) and the region with too-low CRA amplitude in plot on previous slide (high energy). Simulations here have an implicit 1/E spectrum due to the way I sampled energies in the simulation and summed them up in the plots, which is why color distribution doesn’t match the combined trapped + GCR observations.

## Simulation of Omnidirectional Proton Response

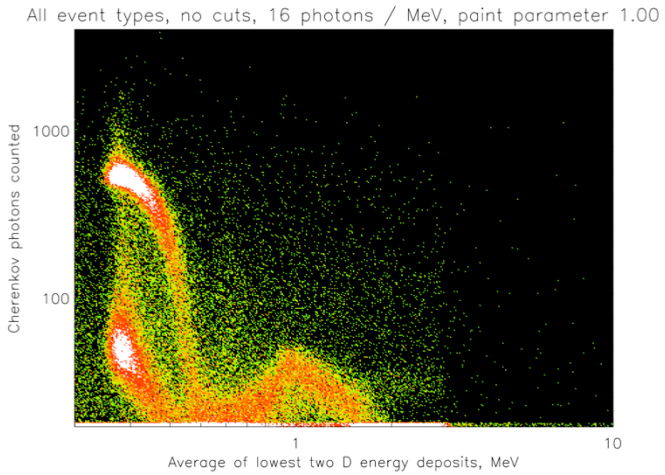


12

AEROSPACE

Here are simulations, again with an implicit 1/E spectrum from the way I sampled energies, showing the omnidirectional proton response of the sensor with a scintillation level of 16 photons per MeV of energy deposit. The "hump" peaking around 1 MeV on the horizontal axis is due to scintillation; the "necks" and "heads" to the left (for higher incident energies, whence lower energy deposits) are the Cherenkov response. The simulations do not pick up the breadth of the response around point B in slide 10, presumably due to greater variability in scintillation output in the real sensor, but the white "wing" matches well. The "heads" labeled A and C on slide 10 are prominent, but the lower one due to backward-going protons is a bit *too* low. We found that adjusting the reflective properties of the black paint placed on the narrow end of the radiator to suppress backward-going response would let us move this around without disturbing the agreement for forward-going protons; the "paint parameter" varies from 1.0 for perfectly absorbing paint to 0.0 for no paint, just a vacuum interface.

## Simulation of Omnidirectional Proton Response

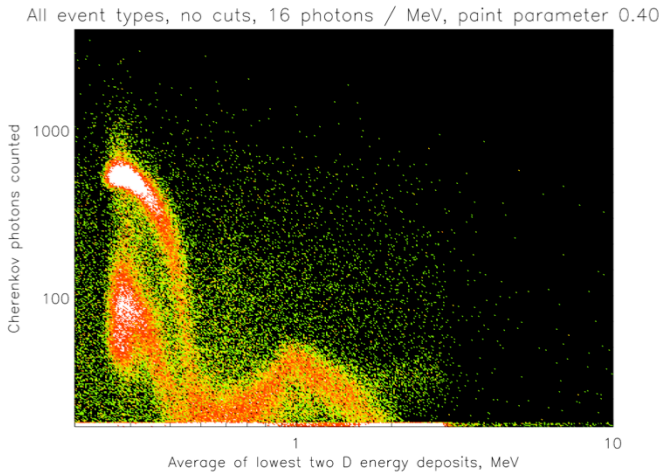


13

AEROSPACE

A “paint parameter” around 0.40 places the “head” C at about the right level and broadens it vertically as observed on slide 10, though comparisons are ongoing. The purpose of this exercise is to quantify exactly the effects of cuts on the response to both forward and backward protons, since (per slide 11) some contamination of the former by the latter is unavoidable.

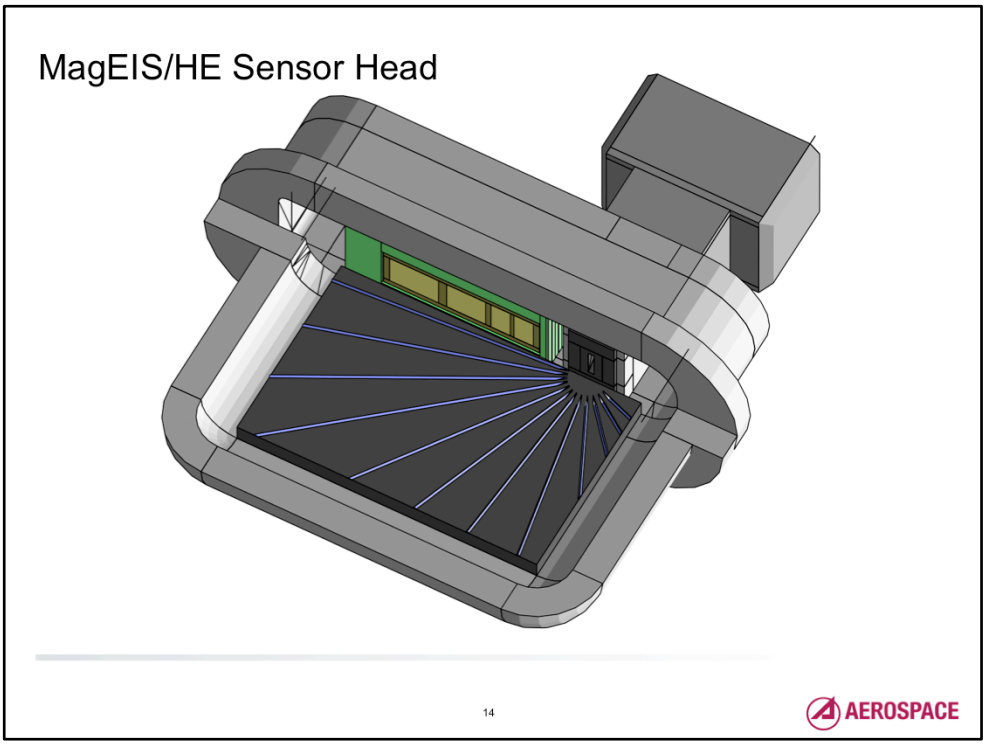


Also aboard the Van Allen Probes are the Magnetic Electron Ion Spectrometer sensors; here we focus on the electron side, which covers three energy ranges: high (pictured here) with a thin front detector and rear detector stack 9 mm thick and a 4800 Gauss field, and medium and low with thinner single detector planes and weaker fields. In previous work we used a rather rickety "toolchain" involving the free version of FASTRAD to read some structures from STEP CAD files via GDML to build a model of the LE head; contrary to what we said at the last Space Users' Workshop, we decided not to continue along that road and instead built this model entirely from Geant4 primitives. The baffles (blue) and magnet gap were particularly difficult; it would help greatly if we could define the magnetic field in a parallel geometry with a simple G4Box instead of dozens of G4Trd objects to define the gap.

## MagEIS/HE Sensor Head, Collimator and Aperture

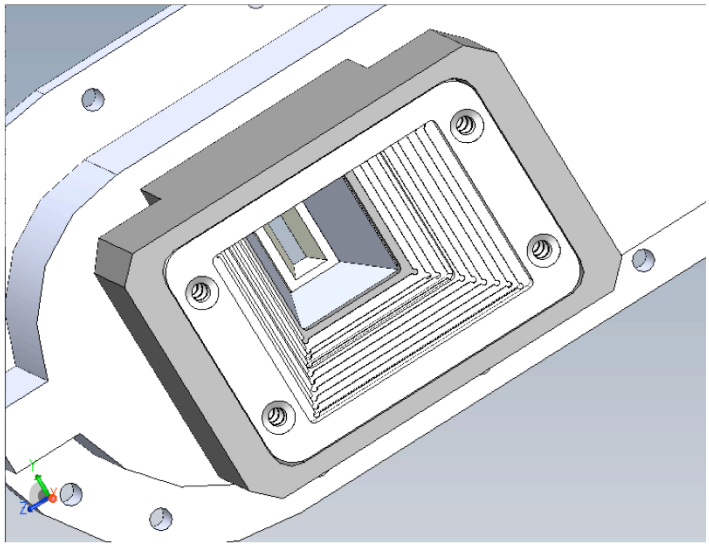

15

AEROSPACE

This is a screen capture from the CAD (eDrawing) file from which I constructed the Geant4 geometry, showing the stainless steel slit with angled shaft above it, and a collimator with tantalum “blades” in front of that. We simulated the omnidirectional response of each of the four pixels to protons and electrons; here we break down the electron response based on where the electron first entered the sensor.

## Simulation of Electron Response

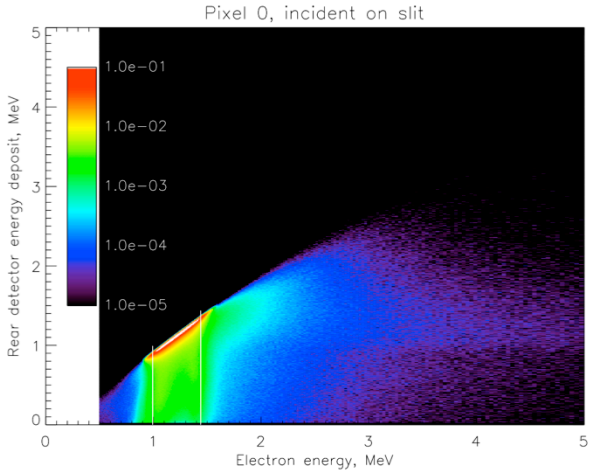


16

AEROSPACE

This is the response of the lowest-energy pixel (nearest the slit) to electrons that actually go directly into the slit, shown as a logarithmic color scale in energy deposit vs. primary energy. The band just below the diagonal is the ideal response; the vertical lines show the energies of electrons traveling in idealized semicircular geometries in a uniform field from the center of the slit to the two edges of the detector pixel. We also see “legs” going down near those limiting energies, where some of the energy deposit leaks out the sides of the pixel, and an “arm” to the upper right that I think is due to particles glancing off the magnets and baffles and striking the “wrong” detector.

## Simulation of Electron Response

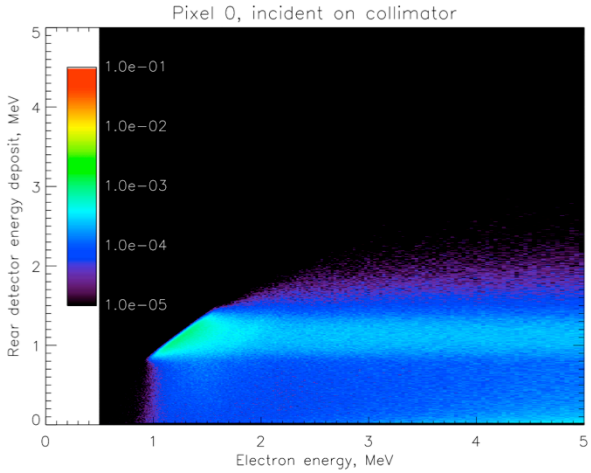


17

AEROSPACE

This is the response of the same pixel to electrons that initially glance off of or penetrate a collimator "blade." These particles lose energy before entering the slit, after which they are sorted into the pixel like any other electron, producing a band that stretches to the right from the location of the ideal response in the previous slide.

## Simulation of Electron Response

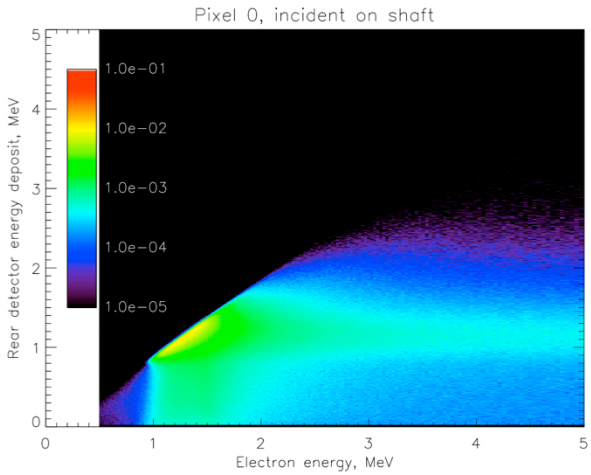


18

AEROSPACE

Response to electrons that first strike the shaft below the collimator is a hybrid of the previous two, since electrons mostly graze the tapered walls and don't lose as much energy as those that actually penetrate collimator blades. We are still working to model the sensor's magnetic field more realistically, notably the effect of stray field up the shaft, but Geant4 provides the ability to model non-ideal effects of scattering of particles into and "leakage" of energy deposit out of each pixel. With pulse height analysis available in the sensor telemetry, we can calculate effective responses and subtract background due to penetrating protons or higher-energy electrons. Geant4 is an indispensible tool for understanding the complex response even of conceptually simple sensors in the real space radiation environment; the biggest challenge for me continues to be selection of physics lists, especially hadronic, though I also have interest in very low energy electromagnetic physics for other projects.


AEROSPACE
Assuring Space Mission Success
© The Aerospace Corporation 2014